Supplementary Information

Imaging protein expression using genetically encoded sensors composed of RNA

Wenjiao Song[1,2], Rita L. Strack[1,2] & Samie R. Jaffrey[1]

[1]Department of Pharmacology, Weill Medical College, Cornell University, New York, NY 10065, USA. [2]These authors contributed equally to this work. Correspondence to: Samie R. Jaffrey (srj2003@med.cornell.edu)

List of supplementary information

SUPPLEMENTARY FIGURE

Supplementary Figure 1. Protein detection and binding saturation curve for RNA sensors

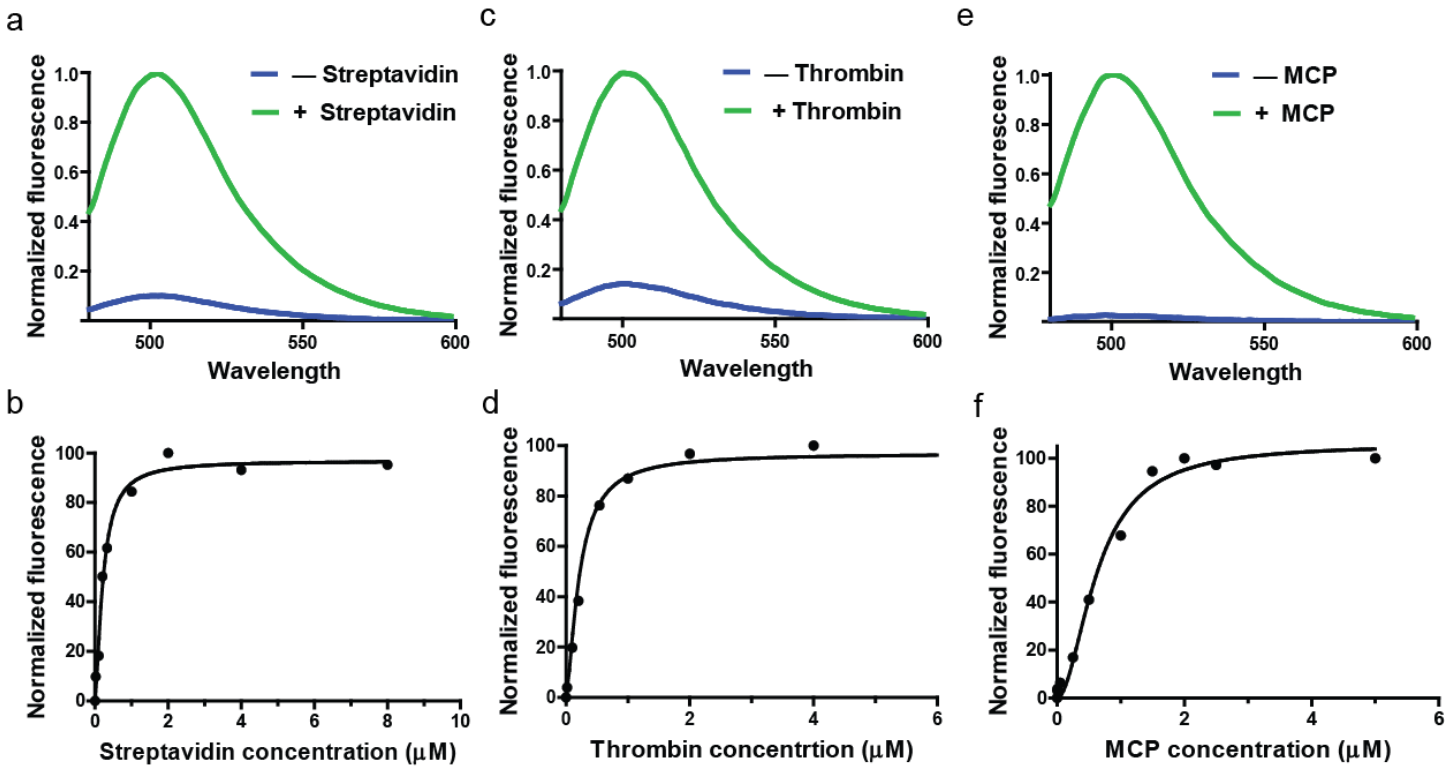

(**a**) Emission spectra of the RNA sensor for streptavidin in the presence or absence of streptavidin. Spectra were collected using 0.2 μM RNA, 10 μM DFHBI and 100 μg/ml (1.7 μM) streptavidin. (**b**) Binding saturation curve for fluorescence detection of streptavidin using 0.2 μM RNA-based streptavidin sensor. (**c**) Emission spectra of the RNA sensor for human thrombin in the presence or absence of thrombin. Spectra were collected using 0.2 μM RNA, 10 μM DFHBI and 40 μg/mL (1.0 μM) thrombin. (**d**) Binding saturation curve for fluorescence detection of thrombin using 0.2 μM RNA-based thrombin sensor. (**e**) Emission spectra of the RNA sensor for MS2 coat protein (MCP) in the presence or absence of MS2. Spectra were collected using 0.5 μM RNA, 10 μM DFHBI and 155 μg/ml (4 μM) MCP. (**f**) Binding saturation curve for fluorescence detection of MCP using 0.4 μM RNA-based MCP sensor

Supplementary Figure 2. The secondary structure and modular design of protein sensors

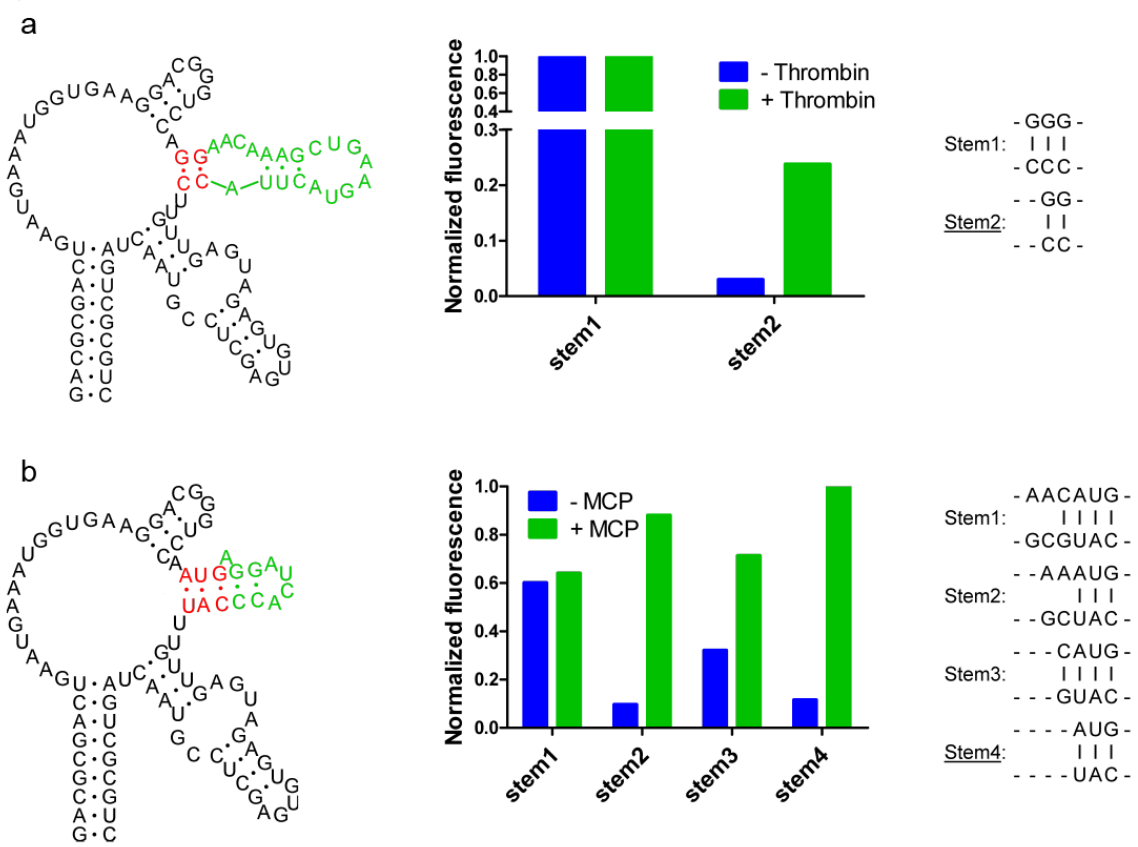

(**a**) The secondary structure and optimization of stem transducer modules for thrombin sensors. The three modular components of the thrombin sensor are depicted. The recognition module (green) constitutes an aptamer that binds to thrombin. The transducer module (red) is composed of two strands which form a weakly base paired stem. Folding of the recognition module upon protein binding juxtaposes the strands in the transducer module, facilitating duplex formation. The Spinach module (black) binds to and activates the fluorescence of DFHBI, but only when the transducer module forms a stem. Two thrombin sensors were generated by fusing the thrombin aptamer to Spinach with two different transducer modules. These transducer modules were chosen because they were predicted to have a very low probability of duplex formation using the secondary structure prediction software Mfold. Thrombin sensors containing different stems (stem 1 or 2) were incubated with 10 μM DFHBI in the presence or absence of 40 μg/ml (1.0 μM) thrombin, and fluorescence emission was measured. (**b**) The secondary structure and optimization of stem transducer modules for MCP sensors. As with the streptavidin and thrombin sensors, different transducer domains were tested for their ability to induce fluorescence in a MCP-dependent manner. MCP sensors containing different stems (stems 1-4) were incubated with 10 μM DFHBI in the presence or absence of 78 μg/ml (2 μM) thrombin, and fluorescence emission was measured. The optimal transducer module (underlined) was chosen because in the context of the sensor it displayed low background fluorescence, with higher fluorescence signal increase upon incubation with proteins.

Supplementary Figure 3. Streptavidin sensor fluorescence in living *E. coli*

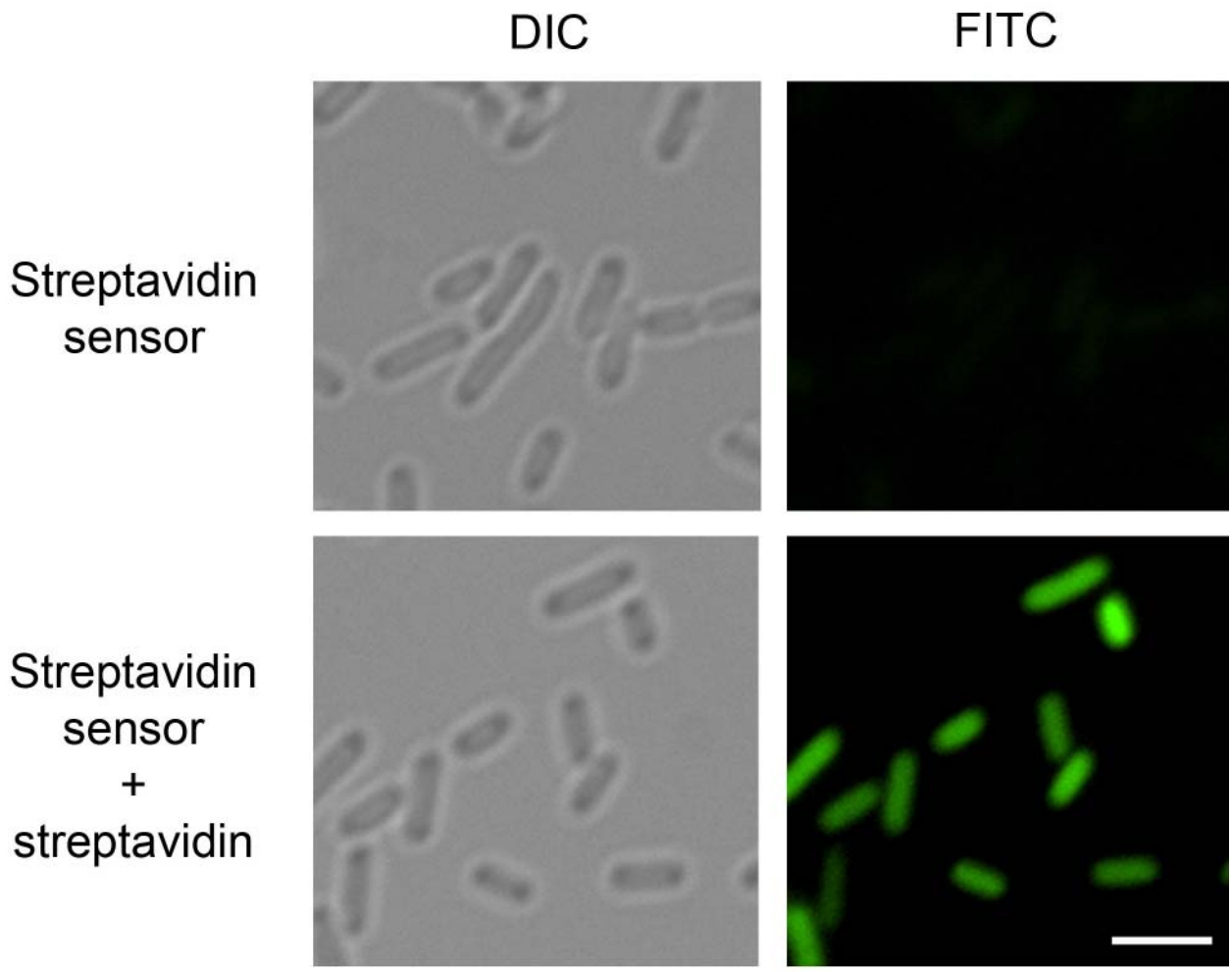

E. coli BL21 cells expressing either the streptavidin sensor alone (top row) or the streptavidin sensor and streptavidin (bottom row) were incubated with DFHBI and imaged. Background signal from untransformed cells incubated with DFHBI was subtracted from green fluorescence. In the absence of streptavidin, very low signal is observed for the streptavidin sensor. However, when streptavidin is coexpressed, the sensor displays approximately 10-fold higher signal, demonstrating that the streptavidin sensor signal is activated by streptavidin binding *in vivo*.

Supplementary Figure 4. Measurement of rate of MCP sensor activation

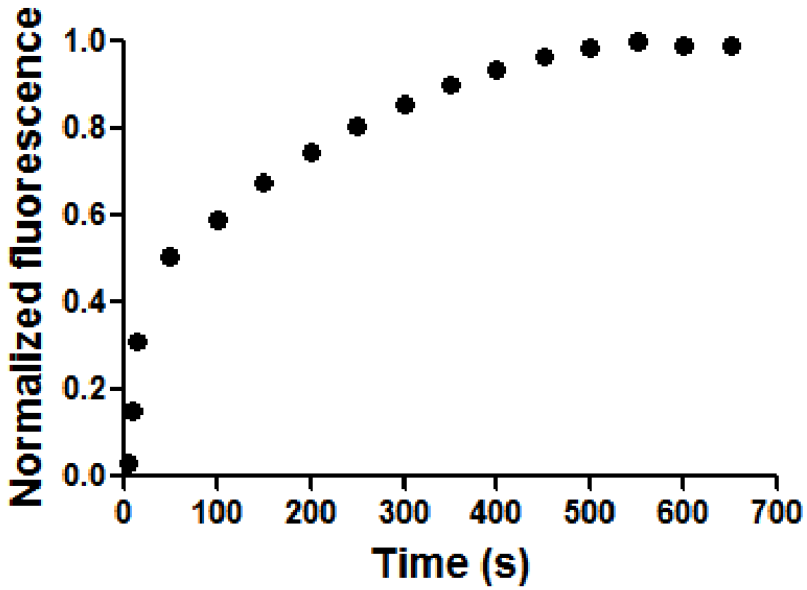

We wanted to know if the MCP sensor rapidly converts to the fluorescent form following addition of MCP. This is particularly important since MCP is synthesized within minutes following MS2 phage infection in *E. coli*. To determine the activation rates, a solution of RNA sensor (10 nM) and DFHBI (10 μM) was incubated with continuous stirring at 25^{o}C in a buffer containing 40 mM HEPES pH 7.4, 125 mM KCl and 50 μM $MgCl_2$. MCP (78 μg/ml, 2 μM) was then rapidly added to the stirring solution and fluorescence emission was recorded over a 15 min period under continuous illumination at 25°C using the following instrument parameters: excitation wavelength, 460 nm; emission wavelength, 501 nm; increment of data point collection, 5 s; slit widths, 10 nm. The fluorescence increase was then plotted against exposure time and normalized to the maximum intensity. We observed rapid signal acquisition for the MCP sensor, with more than half of the total signal appearing after one minute, with maximal fluorescence reached within 8 min.

Supplementary Figure 5. Analysis of MCP concentration after infection

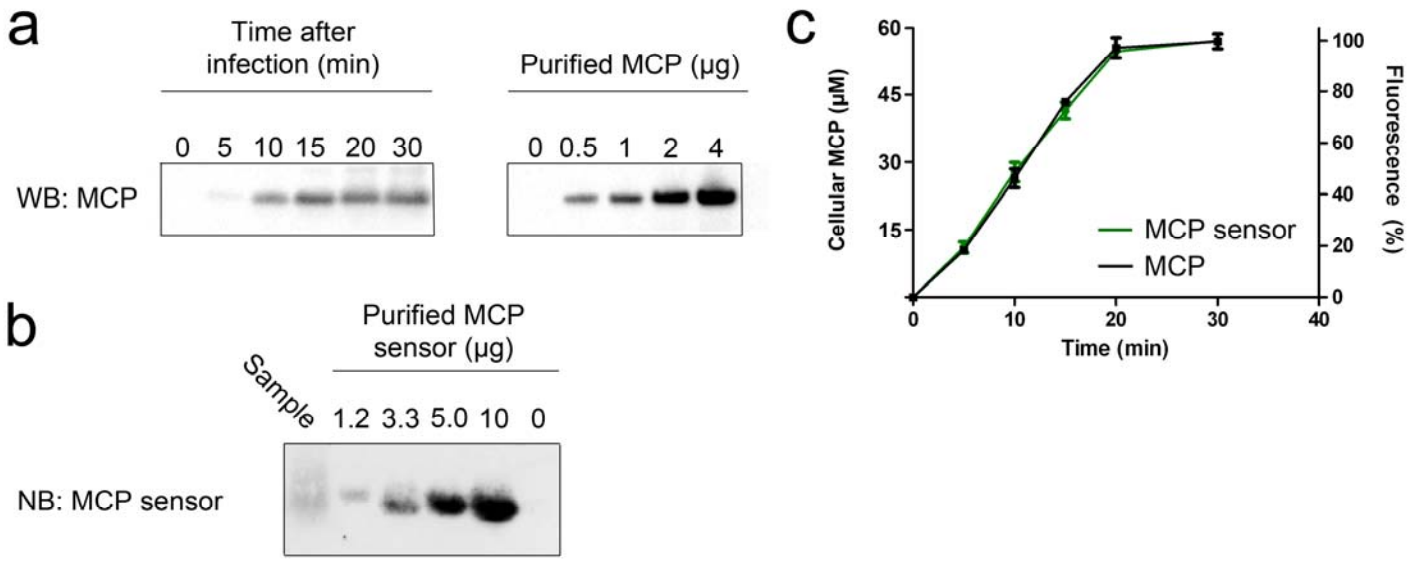

(**a**) MCP synthesis was quantified by western blot analysis. *E. coli* cells were infected at an MOI of 10. At the indicated time points, aliquots were collected and then subjected to western blot with an antibody against MCP (left panel). Purified MCP protein of known concentration was also loaded as a standard on the same blot (right panel). (**b**) MCP sensor levels were quantified by Northern blot analysis. Cellular RNA was extracted from *E. coli* cells expressing the MCP sensor after 2 h induction. Sample and purified controls generated by *in vitro* transcription were run on an agarose gel and subjected to Northern analysis with a probe against the MCP sensor. Sample signal was compared to the standards to determine MCP sensor concentration. (**c**) MCP concentration and fluorescence signal increase linearly over time until a plateau of MCP protein expression is reached. Calculated MCP concentration (black line, left y-axis) correlates perfectly with fluorescence signal from the MCP sensor (green line, right y-axis) and reached a plateau at the same time, confirming that MCP sensor signal does not increase after MCP production has reached a plateau

Supplementary Figure 6. The MCP sensor is specifically activated by MCP produced after viral infection

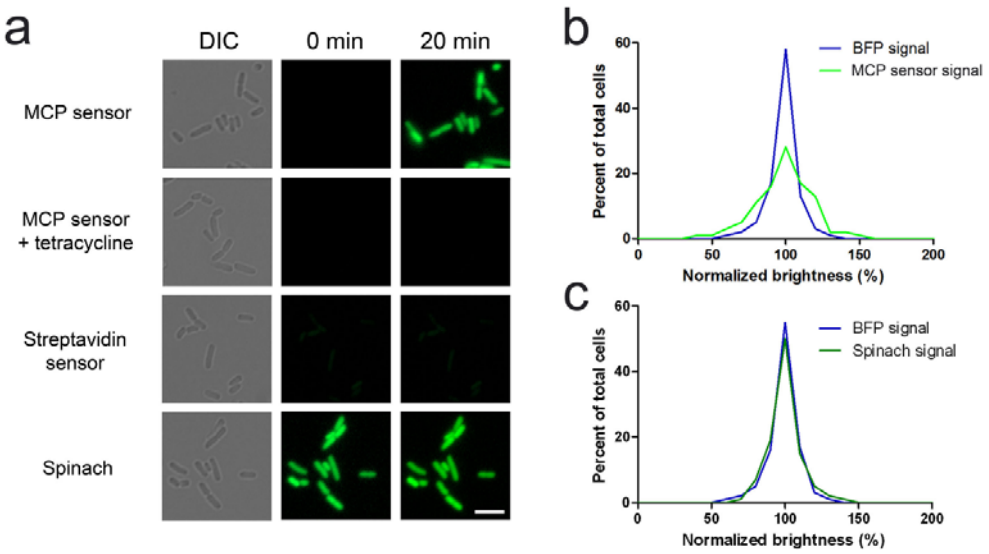

(**a**) Fluorescence in *E. coli* expressing the MCP sensor derives from MCP synthesis. We sought to confirm that the fluorescence seen in *E. coli* expressing the MCP sensor does not reflect nonspecific activation of the MCP sensor. We performed several control experiments to test this. In each experiment, *E. coli* expressing the indicated sensor was infected with MS2 phage at an MOI of 10. *E. coli* expressing the MCP sensor showed background levels of fluorescence before infection, but were brightly fluorescent 20 min after infection (top row). This increase in brightness was inhibited when cells were treated with the protein synthesis inhibitor tetracycline 10 min before and throughout infection (second row). This demonstrates that the sensor is activated by new protein synthesis occurring after infection. This fluorescence increase is specific to MCP production as no fluorescence increase above background was observed in *E.coli* expressing the streptavidin sensor (third row). Importantly, for both the MCP and streptavidin sensor, background fluorescence was minimal, demonstrating that fluorescence is not nonspecifically activated by the cellular environment. Moreover, infection alone does not cause fluorescence increase of the Spinach portion of the sensor, as *E. coli* expressing Spinach exhibited a constant signal throughout infection (fourth row). Exposure times of 500 ms were used for top three rows of fluorescence images, while an exposure time of 100 ms was used for Spinach. Background signal for DFHBI alone was determined by imaging cells harboring an empty control vector under identical conditions and subtracted using NIS-Elements software. Scale bar, 5 μm.(**b**) Expression of MCP sensor is uniform in *E. coli*. In this experiment, we wanted to determine if the expression level of the MCP sensor is uniform in different cells. It is possible that some of the differences in the fluorescence levels seen in Fig. 2a reflect different expression levels of the sensor, rather than different levels of MCP synthesis. To test this, we used a plasmid that expressed both BFP and the MCP sensor, and monitored the variation of BFP expression in cells. We asked if BFP exhibited the same variation as MCP sensor fluorescence following viral infection. In this experiment, *E. coli* were transformed with this plasmid and cells were infected at an MOI of 10 for 20 min. Fluorescence signal in the blue and green channels were then calculated relative to cell volume. The average fluorescence value was set to 100% for each channel, and then cells were binned according to relative brightness. The percentage of cells in each bin is plotted. As shown, BFP signal was very uniform, with greater than 80% of cells within 10% of the average brightness. MCP sensor signal was more variable, indicating that cell-to-cell variability in MCP sensor signal is a direct reflection of differences in MCP synthesis kinetics, and not expression level. The specific cause of this variability, which may relate to stage of cell cycle, age, growth rate, mutations in MS2 phage particles, or other factors, remains to be established(**c**) BFP and Spinach signal are consistent when coexpressed. To confirm that RNA stability does not cause the observed differences in MS2 sensor and BFP signal, Spinach and BFP were coexpressed using the same system and analyzed as described above. BFP signal was very uniform, as previously observed. Spinach signal was also very uniform, and overlaid nearly perfectly with BFP signal. These results support that differences in MS2 infection kinetics, and not RNA stability are responsible for differences in MCP sensor signal compared to BFP.

Supplementary Figure 7. Distribution of cells with respect to MCP synthesis rate.

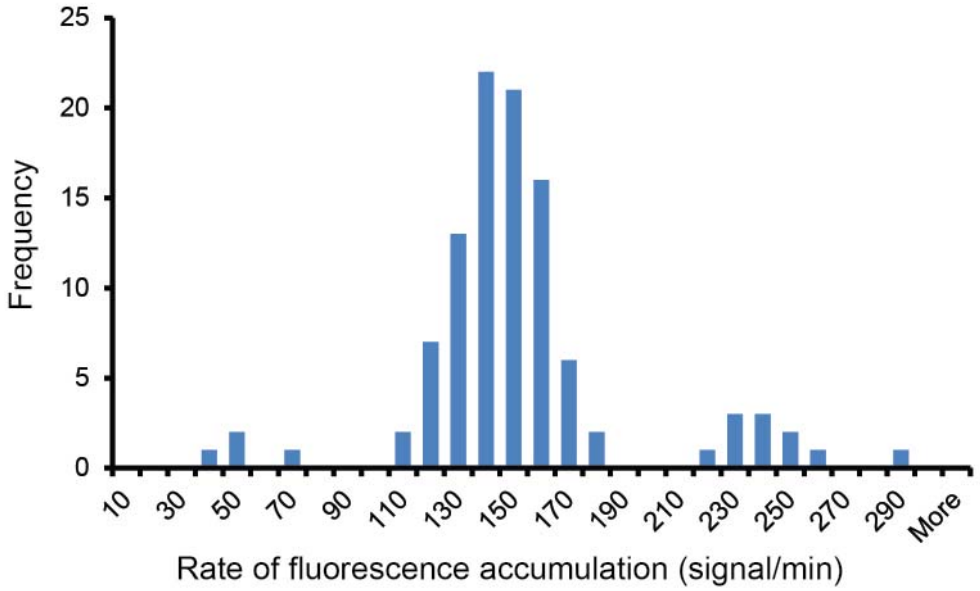

One hundred cells were binned according to the rate of MCP sensor signal increase during the linear phase and plotted as a histogram. The vast majority of cells displayed a normal distribution centered around the average rate. However, two subsets of cells were outliers from the normal distribution, with 11 cells having a faster rate of MCP synthesis, and 4 cells having a slower rate of MCP synthesis.

SUPPLEMENTARY TABLE

Supplementary Table 1. Sequences and binding affinity for RNA-based protein sensors

Sensor	Sequence[a]	Fold activation	Published K_D[b] (nM)
Streptavidin	**GACGCGACTGAATGAAATGGTGAAGGACGGGTCCA** *CGACCGACCAGAATCATGCAAGTGCGTAAGATAGTC GCGGGCCGGGG* **TTGTTGAGTAGAGTGTGAGCTCCGTAACTAGTCGCGTC**	10.3	70
Thrombin	**GACGCGACTGAATGAAATGGTGAAGGACGGGTCCA** *GGAACAAAGCUGAAGUACUUACC* **TTGTTGAGTAGAGTGTGAGCTCCGTAACTAGTCGCGTC**	6.9	0.5
MCP	**GACGCGACTGAATGAAATGGTGAAGGACGGGTCCA** *ATGAGGATCACCCAT* **TTGTTGAGTAGAGTGTGAGCTCCGTAACTAGTCGCGTC**	41.7	0.2
Mutant1	**GACGCGACTGAATGAAATGGTGAAGGACGGGTCCA** *ATGGGGATGTCCCAT* **TTGTTGAGTAGAGTGTGAGCTCCGTAACTAGTCGCGTC**	1	NA
Mutant 2	**GACGCGACTGAATGAAATGGTGAAGGATTCGTCCA** *ATGAGGATCACCCAT* **TTGTTGAGTAGAGTGTGAGCTCCGTAACTAGTCGCGTC**	1	NA

[a]Black bold sequence indicates the Spinach sequence that is used in all sensors. Red italic sequences indicate specific protein binding sequences. Green sequences are mutated regions.

[b]K_D values shown are previously published dissociation constants for RNA aptamers. The K_D for the streptavidin aptamer is taken from supplementary ref. 1. The K_D for the thrombin aptamer is taken from supplementary ref. 2. The K_D for the MCP aptamer is taken from supplementary ref. 3.

This panel examines the specificity of the protein sensors. As an additional control for specificity, a mutant version of the MCP sensor was generated with mutations in the MCP-binding sequence. No fluorescence increase was observed for this mutant in the presence of MCP, indicating that MCP binding to the MCP recognition sequence is required for fluorescence activation. To ensure that fluorescence activation is caused by the induced folding of Spinach, a mutant version of the MCP sensor was also generated with mutations in a crucial stem loop of Spinach. No fluorescence was observed for this mutant, indicating that proper folding of the Spinach portion of the sensor is required for sensor activation. Additionally, as described in the text, the sensors are not activated by the complex intracellular environment in bacteria, further supporting the idea that these sensors are highly selective for their specific targets.

Supplementary Note: Reagents and equipment

Unless otherwise stated, all reagents were purchased from Sigma-Aldrich. Commercially available reagents were used without further purification. Absorbance spectra were recorded with a Thermo Scientific NanoDrop 2000 spectrophotometer with cuvette capability. Fluorescence excitation and emission spectra were measured with a Perkin Elmer LS-55 fluorescence spectrometer.